https://doi.org/10.5194/essd-2026-255
Preprint. Discussion started: 20 July 2026

Open Access Earth System Science Data Discussions

Statewide Forest Monitoring Data for California

Christopher B. Anderson[1,2], David C. Marvin[1,2]

[1]Planet Labs PBC, San Francisco, 94107, USA

[2]Salo Sciences, San Francisco, 94107, USA

Correspondence to: Christopher Anderson (christopher@planet.com)

Abstract.

High severity wildfires, driven by a complex interplay between climate change, vegetation growth, and human activity, present a critical threat to human safety and to the ecosystems of California. Forecasting and managing these fire systems is hindered in part by a lack of comprehensive, long-term, and regularly updated data regarding the vegetation fuel loads and forest structural conditions that drive fire behavior. To address this data need, we developed and launched the California Forest Observatory in the fall of 2020, which is a system designed to map forest structure and fuels at fine spatial and temporal scales. An extensive airborne LiDAR training dataset was integrated with multi-sensor satellite data from Sentinel-1, Sentinel-2, and PlanetScope constellations. LiDAR-derived canopy fuel metrics — including canopy height, cover, base height, and ladder fuel density — were modeled using convolutional neural networks, which leveraged spatial context and sensor fusion to generate predictive models at 10-meter and 3-meter resolutions. Canopy bulk density and surface fuel data were estimated from process-based models. The canopy fuel models demonstrated strong performance: 10-meter model predictions ranged from $r^2 = 0.51$ to $r^2 = 0.79$, 3-meter performance metrics ranged from $r^2 = 0.72$ to $r^2 = 0.79$, with low net bias across all variables, outperforming comparable, recently-released data products. The output data have successfully supported wildfire hazard mapping, utility risk mitigation, and carbon neutrality planning across the state, and are available via PANGAEA (https://doi.org/10.1594/PANGAEA.989871). By providing a data-driven evidence base for monitoring vegetation change, the California Forest Observatory offers a blueprint for the next generation of satellite-based conservation technologies aiming to inform sustainable land management strategies.

1 Introduction

Vegetation-fueled wildfires are a critical part of the Earth system, especially in Mediterranean-climate ecosystems but pose major threats to human populations and built infrastructure, with wildland fires driving significant economic losses, severe air pollution, human deaths, and environmental harm (Bowman et al., 2020; Mietkiewicz et al., 2020). Forecasting severe wildfire dynamics is challenging, stemming from the complex interplay between fire, human activity, vegetation, and climate. Quantifying this interplay is challenging due to a lack of comprehensive historical, long-term, and regularly-updated

https://doi.org/10.5194/essd-2026-255
Preprint. Discussion started: 20 July 2026

data on each component of the fire system. While the need for forest monitoring systems that map multiple dimensions of ecological change is apparent in much of the world, it is especially so in California, a biodiversity hotspot that is home to the oldest and tallest trees, sprawling and lively deserts, and nearly 40 million people (Went, 1955; Myers et al., 2000; Ishii et al., 2008).

California has experienced dramatic environmental changes over the past decade, building on changes that accumulated over the past century. The combination of a mediterranean climate, characterized by frequent droughts and heat waves, and the legacy of cultural burn practices of indigenous Americans, helped establish regular ecological disturbance regimes that maintained biological diversity and mitigated the likelihood of high severity wildfires (Mooney et al., 1974; Salter, 2003; Stephens et al., 2018). The systematic eradication of cultural fire, the implementation of fire suppression tactics, and the appropriation of land for timber and agriculture all dramatically restructured California's forests (Kari Marie Norgaard, 2014; Marks-Block, 2020). Since 1930, for example, tree density has increased by 30% in the state's forests, yet the average tree diameter decreased by 19% over that same period (McIntyre et al., 2015). Forests stocked with small and abundant trees have experienced severe drought stress this past decade, as have the grass and shrublands, leading to the accumulation of dense fuel loads (Diffenbaugh et al., 2015; Schoennagel et al., 2017).

These shifts in forest structure, climate, and management practices underpin a new era of megafire for the state (Linley et al., 2022). According to CALFIRE fire perimeter data, 6,330 fires burned in the period between 2000 and 2019, covering a total of 5.4 million hectares (Fire Perimeters, 2026), representing a significant increase in annual burned area rates from 1900-2000 (Li and Banerjee, 2021). The frequency and intensity of wildfires have increased further this decade, with 2,036 fires burning between 2020 and 2025, covering a total of 3.4 million hectares. Quantifying the patterns of vegetation structure and growth that drive these dynamics, and monitoring their change over time, will be essential for understanding future wildfire exposure and prioritizing fuels management strategies.

The California Forest Observatory — a satellite-based observation system designed to map vegetation fuel distributions, regrowth dynamics and habitat structure across the state — was developed to address the technological and scientific challenges of forest monitoring. The initial data release focuses on wildfire and habitat mapping, two critical priorities for California's conservation and land management planning. In order to support contemporary and legacy wildfire models — including FARSITE, FlamMap, ELMFire and FSIM — all surface and canopy fuel datasets were designed to match the units and definitions of the LANDFIRE fuel and fire behavior products (Rollins, 2009). Several datasets are commonly used in wildlife habitat mapping, including canopy height and canopy cover. In this paper we describe how each dataset was derived, the model performance metrics, and how the data have been used in regional, state, and federal contexts since the data were released in 2020. Designed to quantify the ecological patterns driving environmental and land use policy in California, the Forest Observatory could serve as a blueprint for the next generation of technology-driven ecosystem monitoring tools.

https://doi.org/10.5194/essd-2026-255
Preprint. Discussion started: 20 July 2026

2. Methods

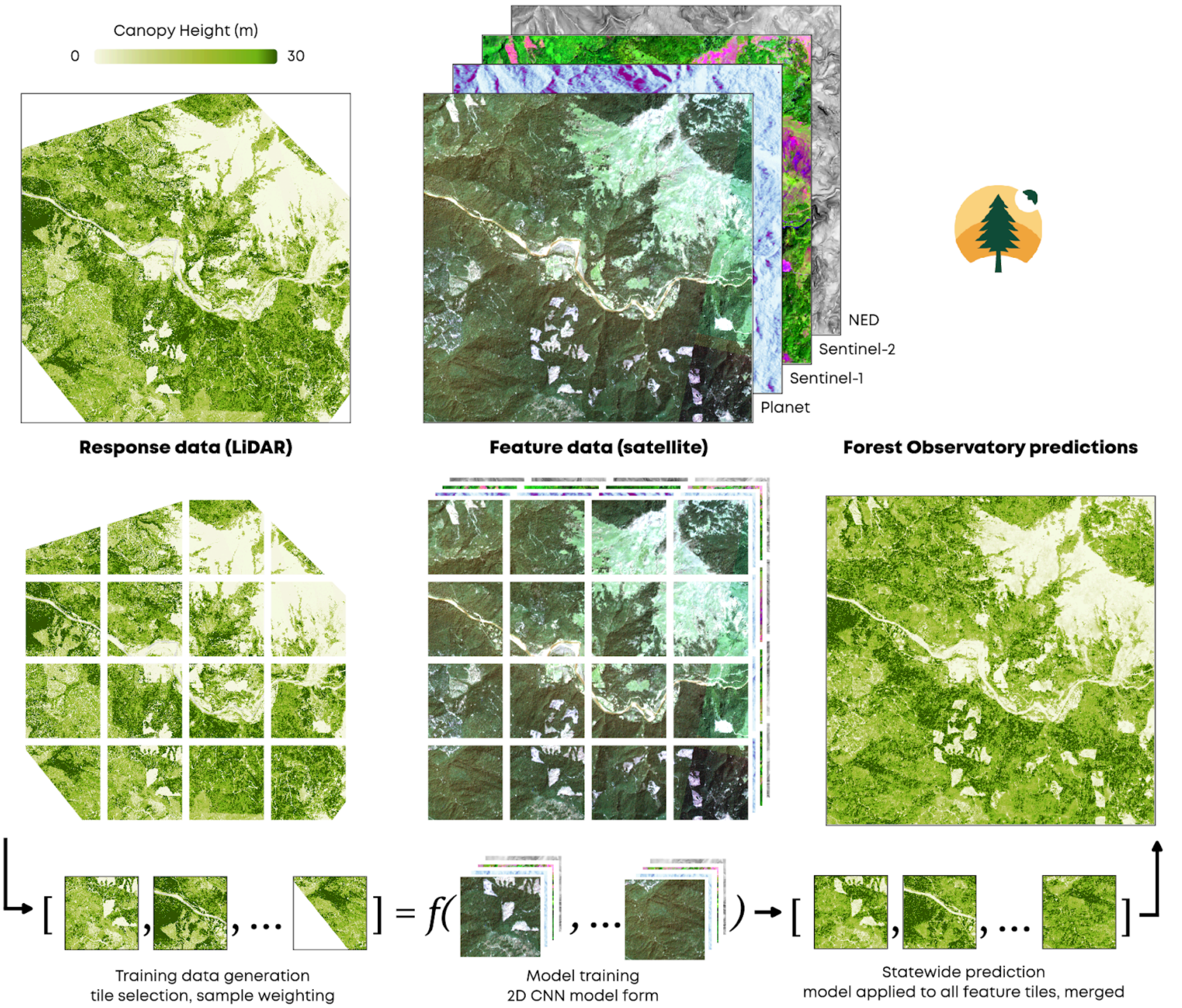

Figure 1: Forest Observatory model training workflow. Publicly-available airborne LiDAR datasets were processed to metrics of forest structure and fuel loads, such as canopy height, which cover limited spatial extents. These data were spatially and temporally co-aligned with multi-sensor satellite imagery, which cover the full extent of California. *n x n* tiles were clipped for each response and feature pair, and a random sample of tiles were used to train 2D CNNs. The trained model was then applied to every feature tile to produce model predictions across the full extent of the state. CNN refers to convolutional neural networks. NED refers to the U.S. Geological Survey's National Elevation Dataset.

https://doi.org/10.5194/essd-2026-255
Preprint. Discussion started: 20 July 2026

The California Forest Observatory integrated multiple data sources and analytical approaches to map and monitor changes in forest structure and fuels over time (Fig. 1). Airborne LiDAR measurements were used as response data, which quantify structure and fuels in fine detail over small extents. Multi-sensor satellite data were used as feature data, sourced from Planet's Dove constellation and the European Space Agency's Copernicus constellations (Malenovský et al., 2012; Planet Labs PBC Team, 2020). These satellite measurements are sensitive to patterns of ecosystem structure and function, and are available contiguously and at regular intervals across the state. Training and covariate data were spatially and temporally co-aligned then used to train Convolutional Neural Networks (CNN) — pattern recognition algorithms that leverage spatial context as predictive features — to develop general LiDAR-satellite relationships. These models were then applied to multi-temporal satellite data to map high resolution predictions of fuel and structure patterns over time. In addition to the forest structure outputs, four additional metrics were derived from process- and rules-based approaches that are described independently.

2.1 LiDAR data

Airborne LiDAR is an active remote sensing technology that can generate detailed, three-dimensional maps of forest structure and terrain, and is extensively used in forestry, geological, engineering and urban planning contexts. LiDAR scanners emit pulses of infrared light at 1064 nm and, since leaves absorb nearly none of this energy due to photoprotection, vegetation reflects or transmits this light in approximately equal proportions, meaning upper, mid and sub canopy vegetation structure can be detected.

An automated data processing pipeline was developed to convert point cloud data into metrics of canopy height, canopy cover, ladder fuel density, canopy layer count and canopy base height. Point cloud data from 47 sites across California were accessed from the USGS 3D Elevation Program (US Geological Survey, 2019), covering a spatial extent of 131,173 km^2 and a temporal extent from 2015 to 2019 (Fig. 2). This processing pipeline was implemented as a series of python routines that wrap LAStools, an open source LiDAR processing library, via a commercial license (Isenburg, 2019).

https://doi.org/10.5194/essd-2026-255
Preprint. Discussion started: 20 July 2026

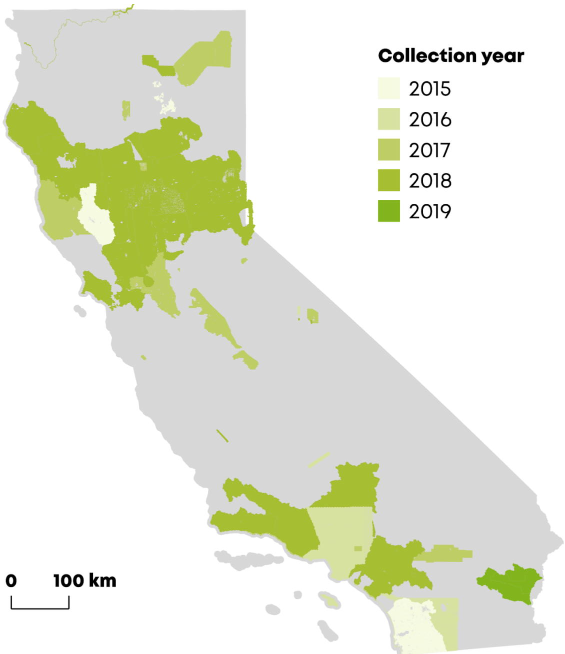

Figure 2: Spatial extents of the LiDAR data used for model training, colored by year of collection.

For each site, the point cloud data were reprojected to the nearest UTM zone and tiled into 1,000 m blocks with 50 m of overlapping buffers to avoid edge triangulation artifacts. Most sites were processed by the provider to include ground point classifications. The few that weren't used all last-return points and a moving kernel, 30 x 30 m in mountainous terrain and 120 x 120 m in urban terrain, to classify ground returns and generate a digital terrain model. The height above ground was then calculated for each point. These height normalized data were used to classify buildings using a planar search function with a 3x3 m kernel and a 0.1 m vertical plane threshold, which identified flat aboveground surfaces (e.g. roofs) as buildings, which were then removed from analysis.

2.2 Forest structure metrics

Canopy height and canopy cover were computed and rasterized at 1 m grid sizes. Canopy height, measured in meters, was calculated as the tallest point within each grid cell. Canopy cover, sometimes referred to as canopy density and measured in percent, was calculated as the number of points above breast height (1.37 m) divided by the total number of points within each grid cell.

https://doi.org/10.5194/essd-2026-255
Preprint. Discussion started: 20 July 2026

Open Access Earth System Science Data Discussions

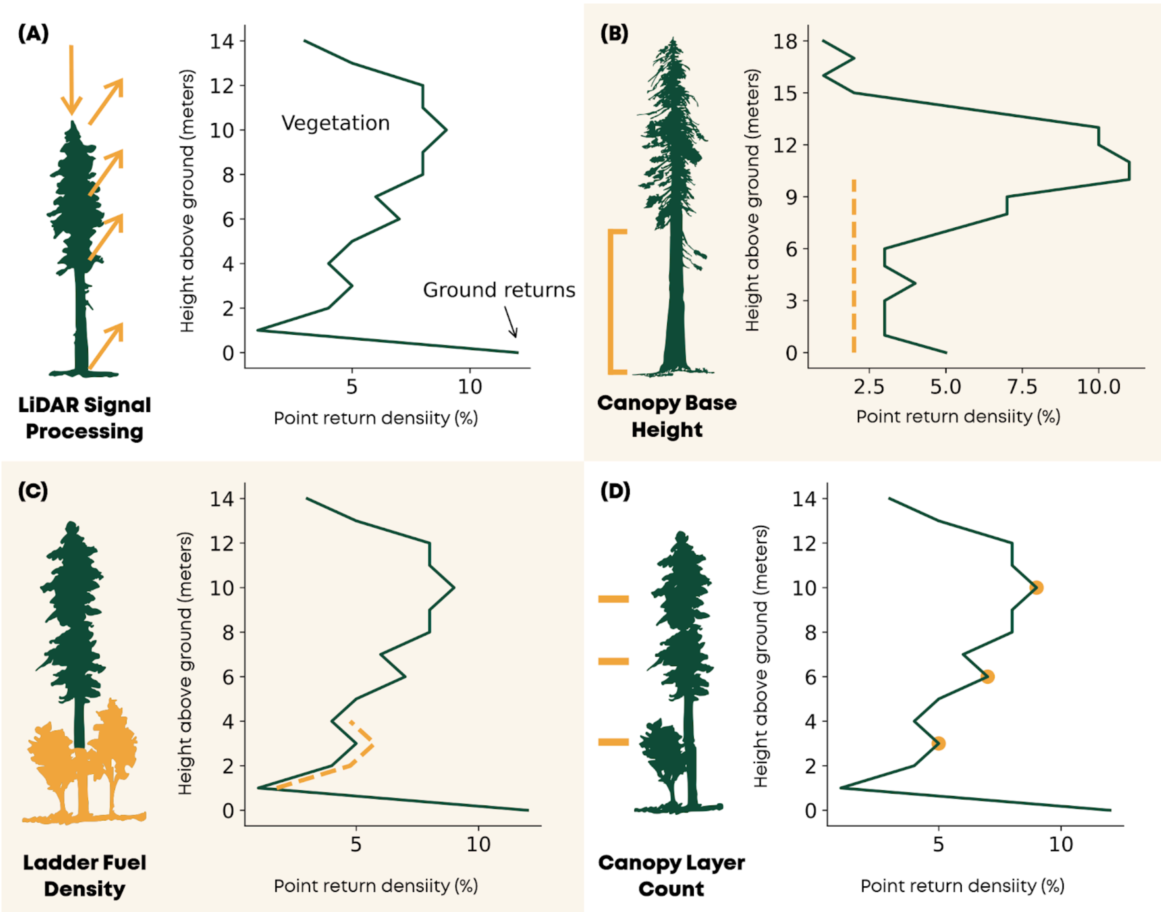

Figure 3: LiDAR processing summary. (A) For each voxel, the number of point returns is normalized across the full voxel to estimate the percent of returns for each vertical meter. This vector is then analyzed to derive metrics like (B) canopy base height, the distance between the ground and the lowest canopy layer, (C) ladder fuel density, the abundance of short (1-4 m) vegetation fuels and (D) canopy layer count, an estimate of the number of unique vertical canopy layers.

Ladder fuel density, canopy layer count and canopy base height were computed using voxel-based analyses (i.e. volumetric pixels) subset to 10 x 10 x 120 m voxels representing (x, y, z_{max}). Canopy voxels subset points along (x, y) horizontal grids and count the number of points within 1 m vertical bins across the range $[0, z_{max}]$. Each bin was then normalized by the total number of returns in the voxel to account for differences in point cloud density between sites. This created a 120-element vector for each voxel, scaled to the density of points within each vertical meter of the canopy (Fig 3). Ladder fuel density, a metric of understory vegetation fuels (Kramer et al., 2014, 2016), measured in percent, was calculated for each voxel per Eq. 1:

https://doi.org/10.5194/essd-2026-255
Preprint. Discussion started: 20 July 2026

$$LFD = \frac{\sum_{i=1}^{4} VD_i}{\sum_{i=0}^{4} VD_i} \cdot 100 \quad (1)$$

Where LFD is ladder fuel density, i is the index of each vertical canopy interval, and VD_i is the density of points within a specific vertical interval.

To compute the number of vertical layers in the canopy, or canopy layer count, we first transformed the voxel density vector into a vertical change detection metric per Eq. 2:

$$C = V_{i+1} - V_i \text{ for } i = \left[0, 1, \ldots, z_{max}\right] \quad (2)$$

Where C is a vector representing the amount of change in canopy density between each progressive vertical layer. Positive values track increases in canopy volume (e.g. increasing branch or leaf density) and negative values track the inverse (e.g. a vertical gap between branches). Canopy layer count was computed as the number of unique, vertically continuous positive C values, including only bins with > 3% positive change. This threshold was applied to reduce noise from LiDAR vertical uncertainty and our choice of voxel bins, as well as to prevent double-counting large, contiguous bunches of vegetation.

Canopy base height (CBH) represents the distance between the ground and the bottom of the canopy. It is intended to be a proxy for the flame length required for a surface fire to transition to a canopy fire, which might also be referred to as the flame gap. Canopy base height is measured as the lowest vertical canopy layer per Eq. 3:

$$CBH = argmin(C \geq 3) \quad (3)$$

Where CBH is the distance between the ground and the lowest layer of the canopy in meters. This represents the lowest vertical position in the canopy where an increase in canopy volume of 3% or greater from the layer below was observed.

2.3 Process- and rules-based models

Canopy bulk density (CBD) describes the mass of available canopy fuel per unit canopy volume that would burn in a crown fire (Van Wagner, 1977; Scott, 2001; Keane et al., 2005). This is calculated as the mass of all leaves and small branches in the canopy divided by the volume that canopy occupies, measured in $kg \cdot m^{-3}$. Equation 4 derives CBD on a per-voxel basis:

$$CBD = \frac{LMA \cdot LC \cdot B}{CH - CBH} \quad (4)$$

https://doi.org/10.5194/essd-2026-255
Preprint. Discussion started: 20 July 2026

Where LMA represents leaf mass per area ($kg \cdot m^{-2}$), LC represents the vertical layer count described above, B is an allometric scalar relating leaf mass to the mass of fine branches in a canopy, CH is canopy height, and CBH is canopy base height. To compute LMA we inverted, rescaled and resampled a global surface leaf area data product from $mm^2 \cdot mg^{-1}$ to $kg \cdot m^{-2}$ (Moreno-Martínez et al., 2018). Since LMA represents leaf mass per horizontal area, we multiplied the leaf mass values by LC to estimate the total leaf mass within a voxel.

In addition to canopy leaves, fine branches also burn in crown fires, and we used allometric relationships defined in the FuelCalc user guide to derive a leaf to branch mass scalar (Reinhardt et al., 2006). The mass of fine branches (i.e. twigs) is typically estimated at ~111% the mass of canopy leaves, and about half the fine branches are typically consumed in crown fires (Reinhardt et al., 2006). To compute the total mass of leaves and half of the branches, we set B to 1.556, which we refer to as the half-twig scalar. To compute canopy bulk density ($kg \cdot m^{-3}$), the total mass of combustible material ($kg \cdot m^{-2}$) is normalized across the vertical space occupied by the canopy, measured in the denominator by the difference between the top of canopy height and the height of the bottom of the canopy (CBH in m).

The fractional cover of photosynthetic and non-photosynthetic vegetation (i.e. green and brown vegetation) were estimated using spectral mixture analysis, providing proxies for grassland fuel density and discriminating between vegetated and non-vegetated areas. Spectral mixture analysis reliably estimates the sub-pixel fractions of green and brown vegetation from multispectral data, and these vegetation fractions correlate directly with field measurements of fresh grass biomass, litter, and standing dead vegetation (Wessman et al., 1997; Asner, 1998; Bateson et al., 2000). To generate statewide green and brown vegetation cover estimates, a spectral unmixing algorithm was developed using a fully-constrained least squares model (Heinz and Chein-I-Chang, 2001). The algorithm estimates the relative abundances of three classes — green vegetation, brown vegetation, and bare ground — using endmembers selected from a global spectral library (Anderson, 2026). A bootstrapped Monte Carlo simulation using 30 random endmembers from each class was used to capture the spectral variance in each class and provide stable unmixing retrievals (Asner and Heidebrecht, 2002). This unmixing algorithm was applied to all Sentinel-2 pixels across all years, providing 5 years of green and brown vegetation cover estimates.

https://doi.org/10.5194/essd-2026-255
Preprint. Discussion started: 20 July 2026

Open Access Earth System Science Data Discussions

Non-Burnable

The first checks determine if the area can carry fire based on infrastructure, land cover, or bare ground.

Third party data:

- Road or Building → **91 (NB1)**
- Cropland → **93 (NB3)**
- Water → **98 (NB8)**

Bare ground:

- Veg Cover < 20% → **99 (NB9)**

Grasses and Shrubs

If **Canopy Height < 5 m** fuel types are defined by vegetation cover and ladder fuel density.

Grasses (Ladder Fuels < 10%):
Determined by **Vegetation Cover** (PV + NPV)

- Veg Cover < 60% → **101 (GR1)**
- Veg Cover 60–75% → **102 (GR2)**
- Veg Cover 75–90% → **104 (GR4)**
- Veg Cover > 90% → **107 (GR7)**

Shrubs (Ladder Fuels > 25%):

- Ladder Fuels < 40% → **141 (SH1)**
- Ladder Fuels ≥ 40% → **145 (SH5)**

Mixed Grass / Shrub:

- Ladder Fuels 10–25% → **122 (GS2)**

Forests and Timber

In forests (**Canopy Height ≥ 5 m**) the understory fuel class is primarily based on ladder fuel density.

Recently burned:

- Time Since Fire < 5 years → **181 (TL1)**

Broadleaf Forest:

- Ladder Fuels < 25% → **182 (TL2)**
- Ladder Fuels 25-50% → **184 (TL4)**
- Ladder Fuels > 50% → **186 (TL6)**

Conifer or Mixed Forests:

- Ladder Fuels < 10% → **185 (TL5)**
- Ladder Fuels > 10% → **165 (TU5)**

Slash / Blowdown:

- Tree cover loss in last 3 years → **202 (SB2)**

Figure 4: Surface fuel model decision tree logic. A series of categorical and continuous variables were used to develop a decision tree for classifying the surface fuel types as defined by Scott and Burgan (2005). Canopy height, ladder fuel density, and vegetation cover were the primary modeled metrics for estimating fuel types, where higher amounts of ladder fuels or vegetation cover correspond to classes that represent heavier fuel loads.

The Scott and Burgan fire behavior fuel model defines around 40 types of surface fuels, which map onto a look up table for a series of parameters like fuel bed depth, dead fuel extinction moisture content, and surface area to volume ratio (Scott and Burgan, 2005). These fuel types are organized hierarchically. Within the Grass fuel type (GR) for example, there are 10 sub-types, GR1-GR9, which are intended to describe the ranges of grass height and grass density that lead to different fire behaviors. The Shrub fuel type (SH) and mixed grass-shrub fuels (GS) describe a range of shrubby vegetation density. Within forests and timber (TU and TL), the sub-types describe broadleaf or conifer forests with varying levels of understory fuel density or recent fire activity. This hierarchical, descriptive organization makes it straightforward to develop a rules-based model to classify fuel types: green vegetation cover provides a good proxy for grass density; ladder fuel density a proxy for shrub or understory density; canopy height can classify forest and timber areas.

Categorical surface fuel data were empirically derived from the forest structure data and from a series of auxiliary datasets using a rules-based process (Fig. 4). The modeled forest structure data, particularly canopy height, ladder fuel density, and vegetation cover, were used to set thresholds to classify the fuel sub-types into classes defined by their overall fuel density. Forest type classifications were extracted from the LANDFIRE 2016 remap product (LANDFIRE, 2016a), and time since fire was calculated using historic fire perimeter data (Fire Perimeters, 2026). One slash fuel type (SB) was used in areas with tree cover loss in the last three years (Hansen et al., 2013), excluding losses within fire perimeters. Several fuel classes were excluded from the model outputs because they are not found in California, such as humid grasses. To map non-burnable areas (NB), reference data were used to classify roads and buildings (OpenStreetMap contributors, 2019), croplands (California Department of Water Resources, 2020), surface water (Hansen et al., 2013), and bare ground.

https://doi.org/10.5194/essd-2026-255
Preprint. Discussion started: 20 July 2026

2.4 Satellite data

We used four satellite earth observations (EO) sources to create our feature data: Sentinel-1 synthetic aperture radar backscatter intensity, Sentinel-2 multispectral surface reflectance, the USGS National Elevation Dataset (NED) elevation model, and Planet multispectral surface reflectance basemaps. Due to differences in spatial resolution (10-20 m for Sentinel, 3 m for Planet) and in data providers, we developed separate preprocessing routines for the Sentinel and Planet data, as well as separate CNN models. All Sentinel and NED mosaics were created using Google Earth Engine (Gorelick et al., 2017) and exported to Google Cloud Platform (GCP). Planet mosaics were built by the Planet Basemap team and accessed via GCP (Planet Labs PBC Team, 2020).

The Sentinel preprocessing pipeline generated cloud-free mosaics for spring and fall over a five year period (2016-2020), co-aligning Sentinel-1, Sentinel-2 and NED data into biannual feature datasets. These multi-year mosaics were generated for three reasons: to introduce inter-annual feature variation to our models, to match the years of LiDAR data available, and because Sentinel data access is constrained by the Sentinel-2A launch in summer 2015. Spring and fall seasonal mosaics were generated for each year (April to June and July to October, respectively), which introduced additional intra-annual feature variation, driven by changes in vegetation phenology and observation conditions (i.e. sun-sensor geometry) between seasons.

For each mosaic, the Sentinel collections were filtered to the dates within each season, composited, masked the areas outside of California, then merged into a multi-band image. The Sentinel-1 raw power-scale image collection was filtered to include just the VV and VH polarizations from Interferometric Wide Swath mode in ascending pass orbits, due to limited or infrequent coverage from descending passes. A mean reducer was applied to compute average pixel-wise backscatter values. Sentinel-2 surface reflectance was filtered to include only the visible, near-infrared and shortwave infrared bands, excluding aerosol and water vapor bands. The collection was masked by removing all pixels with greater than 20% cloud probability prior to compositing to ensure clear observation conditions. NDVI was calculated for each image, and the collection was reduced to a single image by selecting the cloud-free pixels with the highest NDVI to maximize vegetation cover in each mosaic. The Sentinel-1 and Sentinel-2 images were concatenated, along with terrain slope and aspect calculated from NED, and exported to a UTM 10N projection with 10 m resolution. The Sentinel-2 bands with 20 m nominal resolution were resampled via nearest neighbor.

In addition to the Sentinel data, two PlanetScope surface reflectance mosaics were analyzed from fall 2016 and spring 2020. Cloud free, 4-band visible to near infrared surface reflectance basemaps were generated for the state, which were not normalized to account for brightness differences or to visually smooth edges between scenes. The majority of 2016 scenes were sourced from July to November. But since the PlanetScope constellation included fewer satellites at that time, some

https://doi.org/10.5194/essd-2026-255
Preprint. Discussion started: 20 July 2026

snow and cloud cover issues meant a few small regions required imagery from spring 2017. The spring 2020 basemap scenes were sourced from April to May, as there were many more cloud- and snow-free observations over this period. The standard surface reflectance product was selected over the normalized product after preliminary testing, which found lower model performance over a small test region using the normalized product.

2.5 Model architecture

CNNs — U-nets in particular (Ronneberger et al., 2015) — were selected as the primary model form for three reasons. First, it is difficult to consistently derive canopy fuel and forest structure metrics from first principles using satellite EO. While many of the structural and biophysical drivers of canopy reflectance and backscatter are well-characterized, inverting radiative transfer models to map these patterns remains a challenge. Model inversion is often referred to as "ill-posed" in this context because the models are often underdetermined, with more model parameters than can be estimated from the feature data (Combal et al., 2003; Jacquemoud et al., 2000; McCormick, 1992). Estimating forest structure metrics using U-nets offers an empirical alternative to this ill-posed problem.

Second, while many studies have demonstrated the power of pixel-based machine learning EO models, U-nets gain predictive power by quantifying the spatial patterns surrounding each point on the landscape. While spatial ecology has for the most part abhorred relationships of proximity as spatial autocorrelation, an effect that inflates model performance statistics and violates assumptions of sample independence, CNNs instead use contextual information as predictive features. Spatial context is shaped to a large degree by ecosystem processes, including dispersal, species interactions, disturbance history and biogeochemical cycling, which in turn are expressed in the physical structure of an ecosystem.

The third reason relates to multi-scale feature engineering. By applying convolutions to extract contextual information, where kernels aggregate information over multiple spatial scales, U-nets leverage iterative, multi-scale landscape features for predicting local spatial patterns. This is advantageous compared to other methods that perform regressions at a single spatial scale. Most ecosystem patterns are driven by multi-scale processes—acting on genes, species, communities and ecosystems—and including multi-scale features should reduce the risk of overfitting to patterns observed at a single spatial scale (Wiens, 1989; Levin, 1992; Chave, 2013; Anderson, 2018).

In U-net models, a series of encoding layers apply convolutions until the input image tiles become a small image, then decoding layers are added until the spatial dimension matches the initial image resolution (Brodrick et al., 2019; Kattenborn et al., 2021). A Dense U-net form was selected after testing several architectures, where concatenation layers are added between pairs of convolutional layers, constructing rich feature maps that are passed between layers (Zeng et al., 2019). This architecture used 64 x 64 pixel tiles, 64 filters, 3 x 3 convolution kernels, 2 x 2 pooling, a ReLU internal activation function, and a linear output activation function. Mean squared error was the loss function, solved with an Adam optimizer (Kingma and Ba, 2014). A robust (i.e. percentile-based) preprocessing scaler was applied to normalize feature and response data. For sample generation, the LiDAR and satellite data were gridded using 64 x 64 pixel tiles and randomly split into 80/10/10 splits for training, validation, and testing.

Models were fitted independently for each metric. 10 m models using the Sentinel feature data were fitted for canopy height, cover, base height, ladder fuel density, and vertical layer count. Additionally, 3 m models were fit for canopy height and canopy cover, as those were the only layers rasterized at high resolution (the other metrics were derived from 10 x 10 m voxels). The 3 m feature data were 5-band datasets, appending the 10 m canopy height or canopy cover predictions to the 4-band PlanetScope surface reflectance mosaics. This is a form of sensor fusion (Schulte to Bühne and Pettorelli, 2018). By concatenating the predictions from a lower to a higher resolution model, the relevant information from the lower resolution features is propagated to the higher resolution model. Including the lower resolution predictions as a single band also reduced model training time and simplified model inference, providing operational benefits that were critical for reducing cost and runtime.

Once fit, model inference was applied to the annual feature mosaics to produce annual model predictions. For the 10 m models, inference was run for each year from 2016 to 2020. For the 3 m models, inference was run for the bookend years of 2016 and 2020. These statewide raster maps are openly available from PANGAEA (Anderson and Marvin, 2026) and via other cloud-native platforms (see Data availability).

2.6 Evaluating model performance

For the forest structure metrics estimated from airborne LiDAR, model performance was evaluated using the coefficient of determination (r^2), mean absolute error (*MAE*), root mean squared error (*RMSE*), and mean bias. *r2* quantifies the proportion of the observed variance explained by the model predictions. *MAE* provides a straightforward estimate of the average error rate across test data. *RMSE* applies higher penalties to large outliers, and the deviation between *RMSE* and *MAE* provides an indicator of the amount of uncertainty driven by large residual errors. Mean bias does not normalize the absolute error rate but instead computes the average of the overall error rate, helping identify the degree and direction of net bias.

Evaluating the bulk density and surface fuel models is not as straightforward. Canopy bulk density is an important characteristic for predicting crown fire spread, but it is predominantly estimated indirectly and rarely measured in the field (Keane et al., 2005). Without publicly-accessible field data, or standard methods for estimating bulk density from EO data, the bulk density predictions are provided without local validation of the results. And while this challenge was apparent before the data release in 2020, the issue persists; the state of the art remains using process-based models for deriving bulk density estimates without external validation (Martin-Ducup et al., 2025; Pascual et al., 2026). The lack of suitable and open field data is likewise a challenge for classifying surface fuels (Keane, 2013); the surface fuel models are also provided

https://doi.org/10.5194/essd-2026-255
Preprint. Discussion started: 20 July 2026

without local validation. This is understood to be a major challenge and limitation within the field, and the challenge of reconciling field and EO estimates of fuel types has been clearly demonstrated in British Columbia (Baron et al., 2024).

In the absence of suitable reference data for validation, histograms of canopy bulk density and surface fuel values were computed from this random geographic sample and compared to histograms of values from the LANDFIRE 2016 Remap data products (LANDFIRE, 2016a, b). Pixels classified as non-burnable in either dataset were excluded from analysis. These distributions provide direct comparisons of the predicted frequencies of the major fuel types across the state, showcasing the similarities and differences between the fuel products at a population level without making claims regarding the pixel-level accuracy of either data product.

Vegetation cover data, while also derived from process-based models lacking calibration data, can still be evaluated using simulation models. This is done by randomly sampling and averaging a series of reference spectra to simulate mixed pixels, running the unmixing algorithm, then testing the retrieval of the known mixture fractions to the predicted fractions. The retrieval quality resampled to Sentinel-2 bands reported MAE = 9% for green vegetation cover and MAE = 15% for brown vegetation cover (Anderson, 2026). A similar study using full range hyperspectral data reported MAE = 5% for green vegetation cover and MAE = 10% for brown vegetation cover (Ochoa et al., 2025). No additional evaluation was performed.

2.7 Mapping fuel distributions

To visualize ecological and geographic variation in forest structure, a random sample of point locations was used to plot the numerical distributions of each metric across the state. A uniform random geographic sample of three million point locations was selected from across the state, and the 10m canopy fuel predictions from the year 2020 were extracted for each sample. These samples were then grouped according to US EPA Level 3 Ecoregions and plotted as density distributions to showcase ecosystem-scale variation in forest structure across the state (US Environmental Protection Agency, 2013).

https://doi.org/10.5194/essd-2026-255
Preprint. Discussion started: 20 July 2026

3 Results

3.1 Model performance

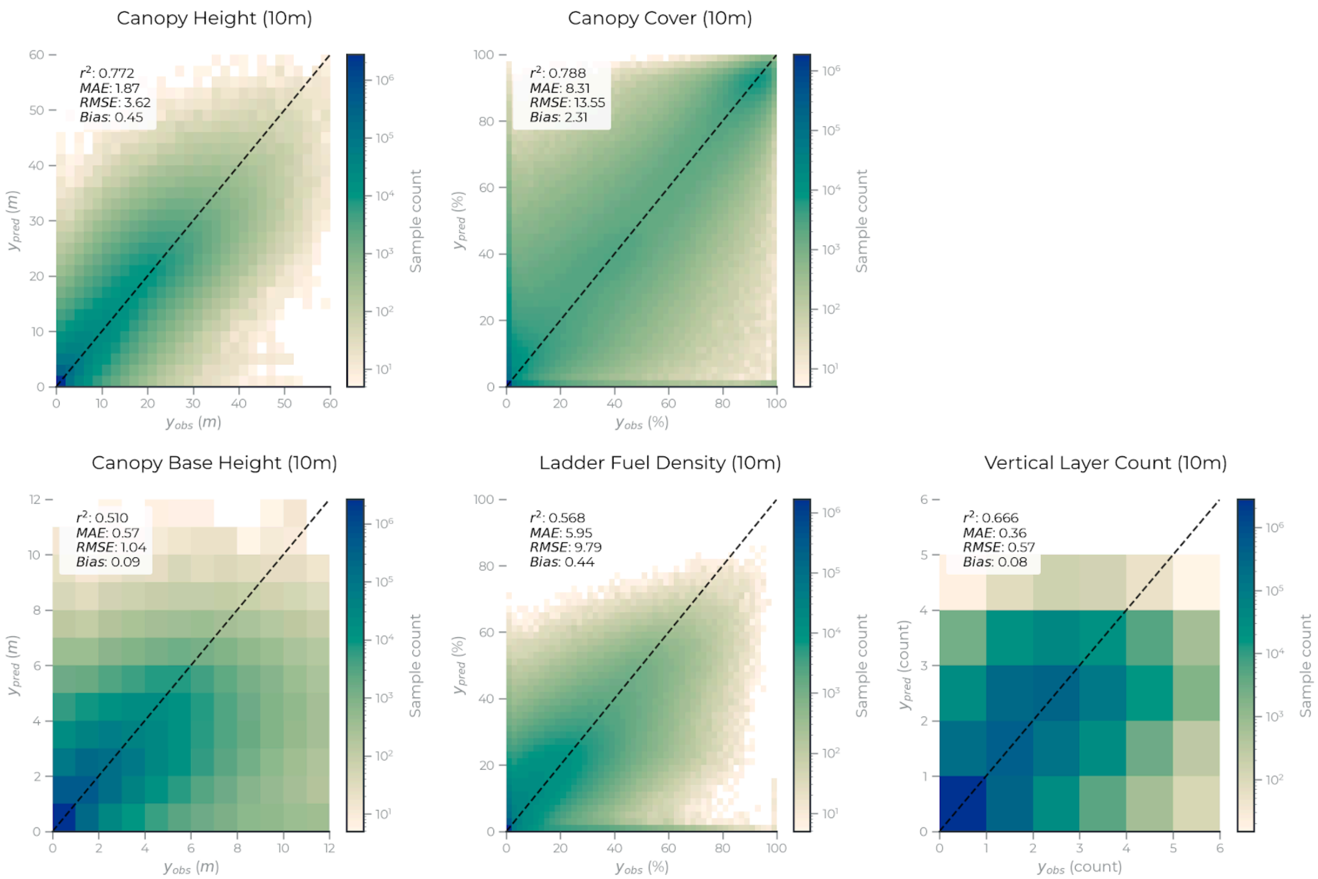

Figure 5: Forest structure regression model performance for 10 m models. 2-D histograms plot the overall agreement between the observed and predicted values of canopy height, canopy cover, canopy base height, and vertical layer count.

Forest structure models fitted at 10 m resolution showed strong performance with low net bias across all metrics on the 10% withheld test data (Fig. 5). The canopy height model reported r^2 = 0.77, *MAE* = 1.9 *m*, *RMSE* = 3.6 *m*, *bias* = 0.45 *m*. Canopy cover reported r^2 = 0.79, *MAE* = 8.3 %, *RMSE* = 13.6 %, *bias* = 2.3 %. Canopy base height reported r^2 = 0.51, *MAE* = 0.6 *m*, *RMSE* = 1.0 *m*, *bias* = 0.09 *m*. Ladder fuel density reported r^2 = 0.57, *MAE* = 5.9 %, *RMSE* = 9.8 %, *bias* = 0.4 %. Vertical layer count reported r^2 = 0.67, *MAE* = 0.36, *RMSE* = 0.57, *bias* = 0.08.

https://doi.org/10.5194/essd-2026-255
Preprint. Discussion started: 20 July 2026

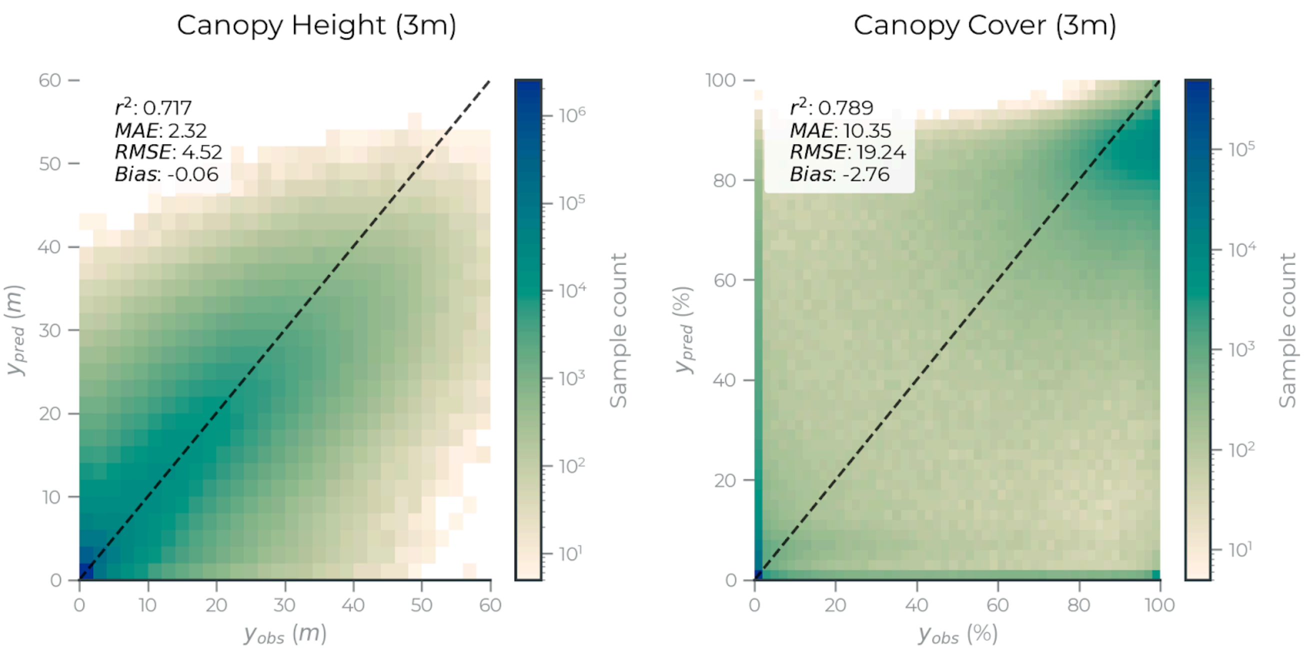

Figure 6: Forest structure regression model performance for 3 m models. 2-D histograms plot the overall agreement between the observed and predicted values of canopy height and canopy cover, the only two variables produced at 3 m resolution.

Forest structure models fitted at 3 m resolution likewise showed strong performance with low net bias, though both metrics report a net negative bias in their predictions (Fig. 6). The 3 m canopy height model reported $r^2 = 0.72$, $MAE = 2.3$ *m*, $RMSE = 4.5$ *m*, $bias = -0.1$ *m*. These metrics indicate slightly lower overall precision compared to the 10 m canopy height model. The same is true to a lesser degree for the 3 m canopy cover model, which reported $r^2 = 0.79$, $MAE = 10.4$ *%*, $RMSE = 19.2$ *%*, $bias = -2.8$ *%*. This decrease in precision coincident with increasing resolution is expected due to the positional uncertainty of PlanetScope scenes, as positional accuracies are reported as less than 10 m RMSE at the 90th percentile, which can result in pixel misalignment between scenes and in comparison to the spatially referenced training data.

https://doi.org/10.5194/essd-2026-255
Preprint. Discussion started: 20 July 2026

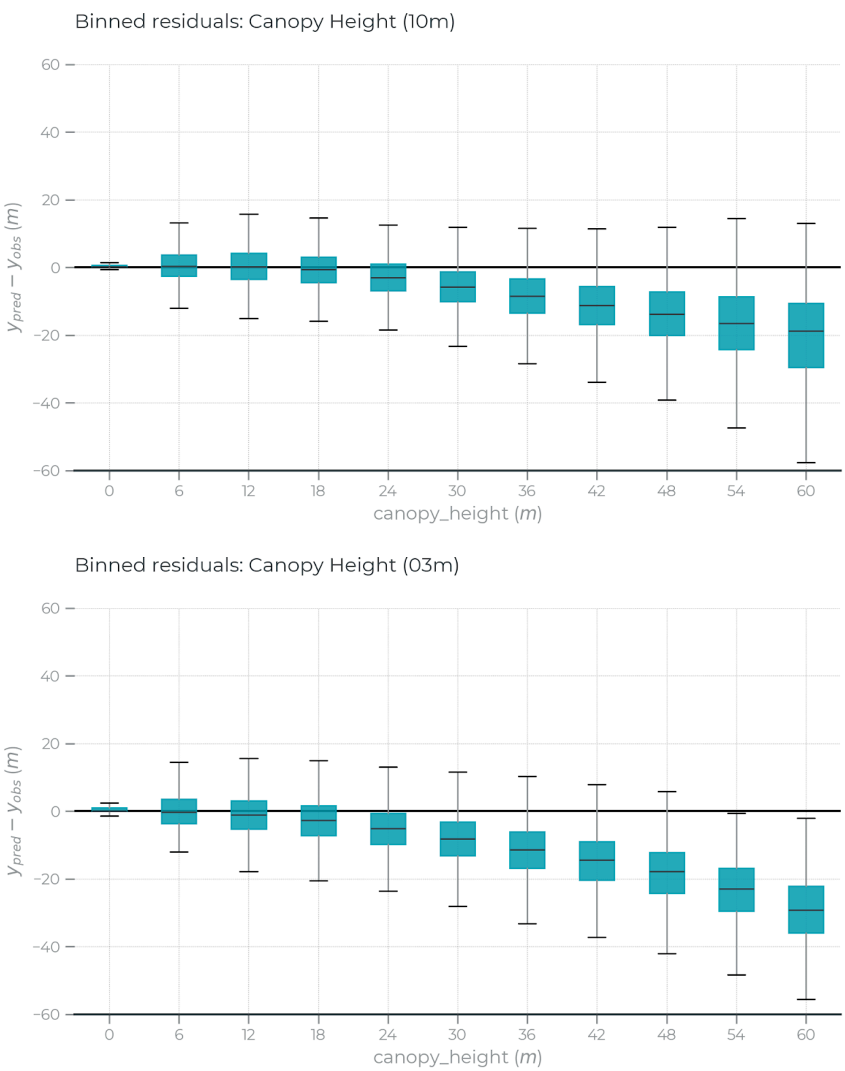

Figure 7: Binned residual plots for canopy height predictions at 10 m (top) and 3 m (bottom) resolutions. Canopy height predictions derived from radar and multispectral covariates often show saturating effects above 20-30 meters, and quantifying the degree of this saturation is important for understanding prediction biases in tall forests.

While the model performance statistics reported low net bias, this does not indicate that bias is uniformly distributed across the range of observed values. The "saturation effect" of limited canopy height retrieval for tall trees is well characterized in vegetation remote sensing (Joshi et al., 2017; Mutanga et al., 2023) and to quantify this effect, predicted canopy height values were grouped according to the observed canopy height and the residual errors are shown in binned residuals plots (Fig. 7). This plot demonstrates the challenge of consistently predicting canopy heights greater than 30 m, with saturation appearing stronger for the high resolution model, with a mean bias of -18 m for observed canopy heights > 50 m for the 10m model, and a mean bias of -21 m for the 3 m model.

https://doi.org/10.5194/essd-2026-255
Preprint. Discussion started: 20 July 2026

3.2 Fuel distributions

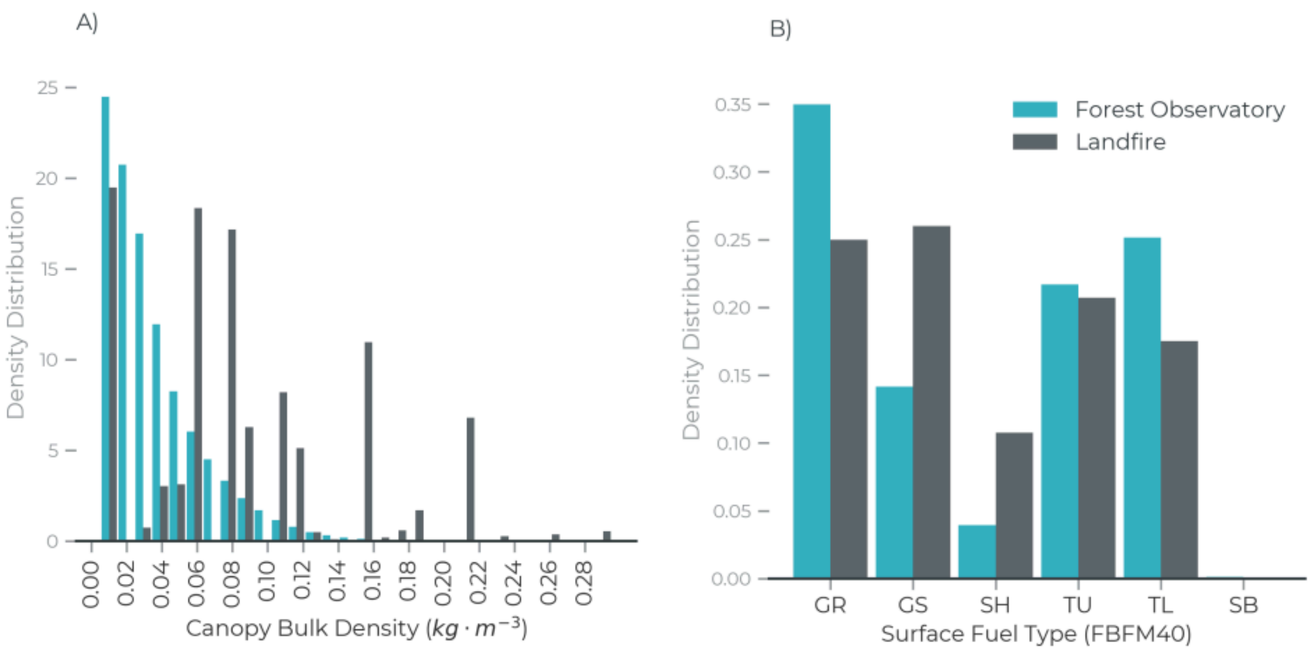

Figure 8: Histograms showing the density distributions of A) canopy bulk density and B) surface fuel model values for Forest Observatory (blue) and LANDFIRE (black) fuels data. A random geographic sample was selected across the state, annotated with canopy bulk density and surface fuel values for each data product. To simplify the comparison, surface fuel classes from the Scott and Burgan 40 fuel models (FBFM40) were aggregated to the major fuel types: (GR) Grass; (GS) Grass-Shrub; (SH) Shrub; (TU) Timber-Understory; (TL) Timber Litter; (SB) Slash-Blowdown.

Frequency distributions comparing canopy bulk density values show lower estimates on average from the California Forest Observatory compared to LANDFIRE (Fig. 8A). The Forest Observatory estimates bulk density as a continuous variable based on a series of remote sensing products, and the values approximately follow an exponential distribution. LANDFIRE on the other hand relies on manual value assignments, resulting in a multi-modal distribution. For surface fuel types (Fig. 8B), the Forest Observatory fuels map a higher proportion of forest types (TU and TL), which is likely the result of using precise high resolution forest structure maps that can map trees outside of forests. Fewer shrub types (GS and SH) are classified in the Forest Observatory, instead mapping more grass fuel types (GR). This is likely the result of using the spatially precise ladder fuels data to only assign shrub fuel classes to the pixels where shrubs occur on the landscape, whereas LANDFIRE typically assigns GS and SH types to broader areas dominated by shrubs.

https://doi.org/10.5194/essd-2026-255
Preprint. Discussion started: 20 July 2026

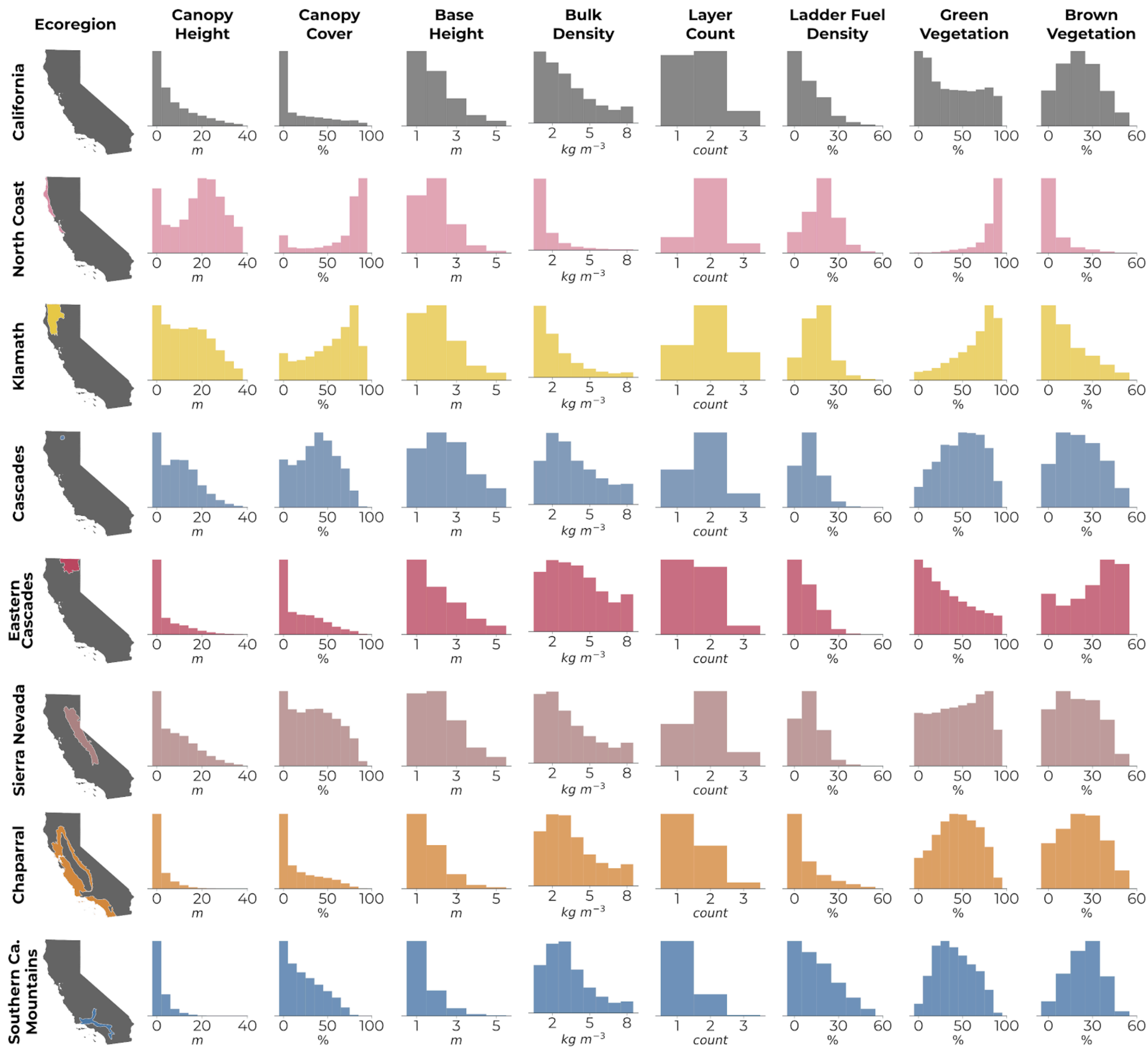

Figure 9: Histograms of eight vegetation metrics across California and within ecoregions. A random geographic sample was selected across the state, annotated with modeled vegetation estimates, and plotted by metric (top). These samples were then subset by ecoregion, and histograms for each metric within that ecoregion show regional deviation from statewide conditions. Only nonzero values for each metric were plotted to minimize zero inflation.

Canopy fuel and vegetation cover data aggregated by ecoregion reveal the distributions of these metrics across ecological systems (Fig. 9). California includes a diverse range of ecosystems that represent gradients of tree cover and structural diversity. At the ecoregion-level, canopy cover was estimated for the Coast Range (72.4%), Klamath Mountains (58.9%), Cascades (41.7%), Sierra Nevada (39.4%), Southern California Mountains (27.4%), Eastern Cascades (23.5%), and South

https://doi.org/10.5194/essd-2026-255
Preprint. Discussion started: 20 July 2026

and Central California Chaparral (21.9%). Sparsely forested ecoregions with less than 15% average canopy cover — the Central Valley and the Central, Mojave, Northern, and Sonoran Basin and Range ecoregions — were excluded from these histograms.

The North Coast is characterized by tall trees, dense understory vegetation, and very high green vegetation abundance, indicating evergreen growing conditions and a complex vertical structure. The neighboring Klamath ecoregion also includes dense canopy cover but deviates from the North Coast with higher proportions of brown vegetation cover and shorter trees. These shifts — represented by shorter vegetation, lower canopy cover, and higher brown vegetation fractions — describe the eastward shifts in drier and hotter climatic conditions in the Cascades and Eastern Cascades. Forest structure metrics in the Sierra Nevada highlight more uniform distributions, indicating a diverse range of ecological states. The Southern California Mountains and the Southern and Chaparral ecoregions are characterized by sparse, shorter trees, lower vertical complexity, shorter base heights, and low green vegetation abundance, representing higher shrub density and high fractions of exposed woody vegetation.

4 Discussion

The release of the California Forest Observatory in 2020 marked an important advance in forest monitoring technologies, enabling open access to multi-year data that quantified multiple metrics of forest structure and vegetation fuels statewide. Though this product was not formally described upon release, this publication provides an opportunity to reflect on the impact the Forest Observatory has made in practice and on how the field has evolved over time.

4.1 Impact

The State of California continues to set ambitious policy goals for reducing wildfire risk, reducing carbon emissions, and safeguarding the environment, often in partnership with the federal government. Ecosystem monitoring technologies can support these policies by providing high quality, up-to-date information on the state of the environment and how it is changing over time (Marvin et al., 2016). The California Forest Observatory was developed to address the multi-agency, multi-stakeholder needs identified in a user engagement process with over 70 participants (Wolff et al., 2020). One key need that emerged was for high resolution, high quality maps of forest structure, fuel loads, and wildfire hazard that can be aggregated to community and regional scales to drive comprehensive hazard mitigation, prioritize forest restoration, and support planning policies to reduce emissions from catastrophic wildfires.

Once released, Forest Observatory data were integrated into data-driven dashboards and resource assessments used to inform state and federal planning. For example, it was used to construct a database of contemporary reference sites in the Sierra Nevada to help design and evaluate ecologically centered management treatments in the ecoregion (Chamberlain et al.,

https://doi.org/10.5194/essd-2026-255
Preprint. Discussion started: 20 July 2026

2023). A series of raw and derivative data products quantifying forest structural heterogeneity and large tree density were included in US Forest Service's Sierra Nevada Regional Resource Kit, which helps land managers assess their landscape and plan for treatments to enhance resilience to human and natural disturbances (Young-Hart et al., 2024). The Tahoe Central Sierra Initiative derived gap fraction and fractal dimension estimates, two metrics of forest structural heterogeneity (Jeronimo et al., 2019), which were used to evaluate current, future, and target conditions under different land management strategies and disturbance regimes to define a Blueprint for Resilience (Manley et al., 2023). The Nature Conservancy used the data to estimate restoration outcomes by quantifying gap sizes driven by fuel reduction treatments (Hendershot et al., 2026). In their Scoping Plan for Achieving Carbon Neutrality, the California Air Resources Board used Forest Observatory canopy cover and ladder fuel density data to quantify defensible space for every parcel in the state and simulate the emissions impacts of enforcing defensible space regulations statewide (California Air Resources Board, 2022).

Comprehensive wildfire hazard mitigation in California critically depends on quantifying and reducing risks attributed to utilities assets, and utilities have invested billions of dollars in risk mitigation activities over the past decade (Singh et al., 2025). With vegetation-driven fires accounting for over 50% of power line ignitions — driven primarily by branch falls, tree failures, and prolonged contact with distribution wires — data that maps where trees might contact power lines provides critical insights into potential ignition sources. Wang et al. (2023) used the data to quantify utility wildfire risks and identify key equity considerations relating income inequality, wildfire exposure, and electricity rates. One study combined Forest Observatory with weather, topographic, and utility infrastructure data to develop machine learning models that predict ignition probabilities, finding tree height was consistently among the top predictors of vegetation-driven ignitions (Yao et al., 2022). Prior to — and independent of — the Yao et al. study, PG&E developed a similar statistical model to quantify vegetation-driven ignition probabilities, deriving more complex features like strike tree classifications and strike tree density, and this model has been codified into their Wildfire Risk Mitigation Plan (Pacific Gas & Electric, 2024).

High resolution forest structure data provides key insights for domains beyond wildfire. The California Forest Observatory has been frequently used to quantify wildlife habitat, particularly for avian species. For example, the California Spotted Owl (*Strix occidentalis occidentalis*) is an old forest-dwelling owl, and preserving their habitat is a high conservation priority. Forest Observatory data have been used to show that tall, heterogeneous forests improve prey capture and reproductive success (Wilkinson et al., 2023; Zulla et al., 2023), to discriminate between spatial and acoustic home ranges to simplify rapid and adaptive monitoring surveys (Gustafson et al., 2025; Kramer et al., 2024), and to model expected range shifts for the Barred Owl (*Strix varia*), an invasive apex predator that threatens Spotted Owls (Watson et al., 2024). Other studies used the data to reinforce the importance of forest structural heterogeneity over management regime in promoting Olive-sided Flycatcher (*Contopus cooperi*) occupancy (Hack et al., 2024), to identify that fine-scale structural complexity facilitates Pacific martens (*Martes caurina*) foraging while reducing predation risk (Delheimer et al., 2023), and to quantify bird community diversity in service of understanding human-avian interactions in urban communities (Langhans et al., 2025).

https://doi.org/10.5194/essd-2026-255
Preprint. Discussion started: 20 July 2026

Open Access Earth System Science Data Discussions

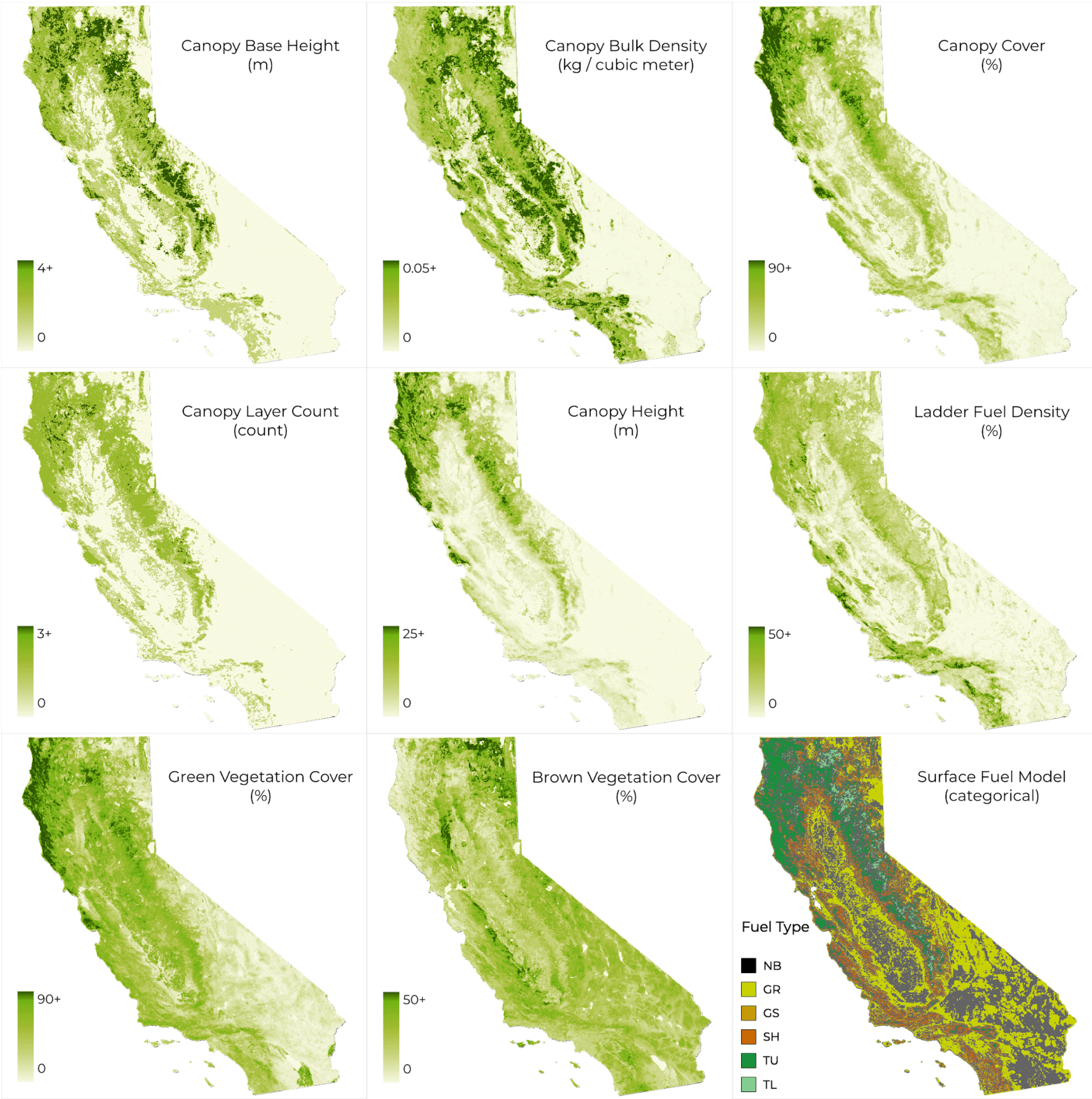

Figure 10: Statewide maps for 9 vegetation data products. Maps were rendered with average spatial resampling, reducing the dynamic range of values represented at statewide aggregations. Surface fuel types: (GR) Grass; (GS) Grass-Shrub; (SH) Shrub; (TU) Timber-Understory; (TL) Timber Litter.

https://doi.org/10.5194/essd-2026-255
Preprint. Discussion started: 20 July 2026

4.2 Forest monitoring data in California

While there have been major advances in geospatial AI over the past several years, particularly related to geospatial foundation models (Zhu et al., 2026), the California Forest Observatory data products still represent a high water mark in terms of model performance. The 10 m canopy height model here reports *MAE = 1.87 m* and *RMSE = 3.62 m*, while a comparable product derived from aerial imagery reported *MAE = 3.42 m* and *RMSE = 6.1 m* when aggregated to 10 m resolution (Wagner et al., 2024). Another product derived from aerial imagery and a vision transformer model reported $r^2 = 0.69$ when aggregated to 15 m resolution (Chang et al., 2025), and a super resolution product from the same group reported an aggregated $r^2 = -0.62$ (Ndegwa et al., 2026), both of which are lower than $r^2 = 0.77$ and $r^2 = 0.72$ for the Forest Observatory models at 10 m and 3 m resolutions without aggregation. Canopy height saturation is less pronounced for Forest Observatory data than other data products, as Ndegwa et al. (2026) showed mean biases of -21 m, -25 m, and -30 m across multiple data products for trees >= 50 m tall, whereas the results here report a mean bias of -18 m for trees >= 50 m tall. Each of the above comparisons rely on reported statistics from each paper, not independent analyses performed here. These results demonstrate that canopy height models fitted using multi-sensor, multi-temporal satellite data and a large, geographically diverse collection of airborne LiDAR data can operationally generate high quality forest structure estimates and regularly update these estimates over time with new satellite observations.

Beyond the quality comparisons, the California Forest Observatory was unique in mapping not only canopy height, but nine separate metrics of forest structure and vegetation fuels, provided over a five year time span (Fig. 10). The integration of both optical and radar data reduced prediction uncertainty and helped retrieve more complex metrics like canopy layer count, since radar observations are sensitive to vertical canopy structure and less sensitive to seasonal foliar variation than multispectral data (Konings et al., 2019). Prediction stability poses a major challenge for mapping forest structure over time, however, often requiring post-processing approaches to generate reliable estimates of change (Turubanova et al., 2023). Such post-processing was not applied to this data product, which poses challenges to interpreting year-over-year prediction variation. Regardless, the level of detail provided by multiple structural metrics allowed users to represent complex patterns of wildfire hazards and wildlife habitat over time, which proved useful for quantifying pre-fire conditions just before the 2020 fire siege and the major fire seasons that have followed.

Like many operational products, several outstanding issues were identified but not addressed prior to the initial release. Year-over-year prediction variability, driven by both varying observation conditions and model uncertainties, made it challenging to rigorously compare annual changes in forest structure. The models did not generalize particularly well outside of California, an indicator of overfitting to local features. User adoption was slower than anticipated because the data products had not yet been peer reviewed, fueling skepticism regarding quality. Additional funding to continue operational production and maintenance was not immediately forthcoming. Navigating these scientific, technical, and organizational

https://doi.org/10.5194/essd-2026-255
Preprint. Discussion started: 20 July 2026

challenges defined the years that followed the release of the California Forest Observatory, and the lessons learned have now been encoded in a series of global data products developed by Planet for mapping forest structure and aboveground biomass over time (Anderson et al., 2025).

5 Conclusions

California faces multiple pressing environmental and policy challenges related to forest management, especially regarding tradeoffs in management objectives between increasing wildfire resilience and decreasing carbon emissions (Herbert et al., 2022). While simulation models show it is possible for improved land management to contribute to each of these objectives and meet net neutrality goals (Sleeter et al., 2019), there remains a need for operational, state-wide forest monitoring systems to quantitatively evaluate progress and to identify and avoid reversals (Badgley et al., 2022; Coffield et al., 2022). The California Forest Observatory represents an example of how such a system could be deployed in practice. Its goal was to provide a data-driven evidence base to quantify changes in forest structure and vegetation fuel loads over time, revealing the downstream effects of those changes to the multiple stakeholders responsible for stewarding sustainable land management practices across the state, particularly for wildfire and wildlife management.

In her book on Digital Earth technologies, Bakker (2024) cited the California Forest Observatory as an ambitious, well-designed technology system that could help optimize fire prevention strategies, improve firefighting situational awareness, and save lives through reducing wildfires caused by aging electricity infrastructure. Forest Observatory data have been used for all of these purposes; never as a sole resource, but as a part of an array of technologies that agencies, utilities, and communities use to map, monitor, and manage the complex dynamics of wildfire across the state. Bakker posited that the responsible use of Digital Earth technologies depends on transparency, credibility, accessibility, and the ability of communities to maintain control over the data and narratives they hold. The Forest Observatory was developed to align with such paradigms of responsible technology design, and we look forward to further advancing evidence-based land management policies with satellite technologies.

Appendix A: LiDAR source data

Table A1. Source data for airborne LiDAR data accessed from USGS 3DEP.

Site	Year	Area (km^2)
CA_Burney_Lassen_2015	2015	444
CA_Central_Valley_2017	2017	2911
CA_Duvall_SantaCruz_2017	2017	45
CA_E_SanDiegoCo_2016	2016	3905

https://doi.org/10.5194/essd-2026-255
Preprint. Discussion started: 20 July 2026

CA_FEMA_R9_Alpine_2017	2017	66
CA_FEMA_R9_Cow_Creek_2017	2017	292
CA_FEMA_R9_Keefer_2017	2017	255
CA_FEMA_R9_Mendocino_HF_2017	2017	3426
CA_FEMA_R9_Russian_2017	2017	1597
CA_FEMA_R9_Upper_Pit_2017	2017	4126
CA_Klamath_Topography_2018	2018	250
CA_Klamath_Topography_TL_2018	2018	48
CA_Krugh_SSierra_2016	2016	252
CA_LTBMU_East_2018	2018	1018
CA_LTBMU_West_2018	2018	492
CA_LakeCounty_2015	2015	3671
CA_LongValleyCaldera_2017	2017	355
CA_LosAngeles_2016	2016	10786
CA_Martens_Yosemite_2016	2016	57
CA_Montecito_2018	2018	198
CA_NoCAL_Wildfires_B1_2018	2018	7305
CA_NoCAL_Wildfires_B2_2018	2018	10555
CA_NoCAL_Wildfires_B3_2018	2018	6935
CA_NoCAL_Wildfires_B4_2018	2018	6157
CA_NoCAL_Wildfires_B5a_2018	2018	6117
CA_NoCAL_Wildfires_B5b_2018	2018	4604
CA_NoCAL_Wildfires_PlumasNF_B1_2018	2018	4236
CA_NoCAL_Wildfires_PlumasNF_B2_2018	2018	5077
CA_NoCal_Wildfires_B5b_2018	2018	1567
CA_NoCal_Wildfires_CampFire_2018	2018	764
CA_NoCal_Wildfires_GMEG_2018	2018	794
CA_Riverside_B1_2019	2019	1473
CA_Riverside_B2_2019	2019	2763
CA_SE_Fault_Zone_2017	2017	2211
CA_Sacramento_2017	2017	3395
CA_SanDiegoQL1_2014	2014	44
CA_SanDiegoQL2_2014	2014	2748
CA_SanDiego_C17_2015	2015	4227

https://doi.org/10.5194/essd-2026-255
Preprint. Discussion started: 20 July 2026

CA_Sare_Mammoth_2018	2018	24
CA_SoCAL_Wildfires_TL_2018	2018	110
CA_SoCal_Wildfires_B1_2018	2018	7910
CA_SoCal_Wildfires_B2_2018	2018	5807
CA_SoCal_Wildfires_B3_2018	2018	7278
CA_SoCal_Wildfires_B4_2018	2018	3480
CA_Sonoma_A3_2013	2013	892
CA_Vadman_CentralCoast_2018	2018	79
CA_WestCoastElNinoUTM11_2016	2016	377

Data availability

The California Forest Observatory data are available at PANGAEA: https://doi.org/10.1594/PANGAEA.989871 (Anderson and Marvin, 2026)

For cloud-native access to the data using modern geospatial software, the data are hosted in publicly-accessible cloud storage, and a STAC catalog is available at the following URL: https://storage.googleapis.com/cfo-public/catalog.json

This catalog can also be accessed from STAC Index: https://stacindex.org/catalogs/forest-observatory#/

Author contributions

CA and DM jointly conceived the ideas, designed methodology, collected data, and analyzed data. CA led writing of the manuscript, and DM contributed critically to the drafts and final manuscript.

Competing interests

The authors are current employees and shareholders of Planet Labs PBC.

Disclaimer

The findings and views described herein do not necessarily reflect those of Planet Labs PBC.

https://doi.org/10.5194/essd-2026-255
Preprint. Discussion started: 20 July 2026

Copernicus Publications remains neutral with regard to jurisdictional claims made in the text, published maps, institutional affiliations, or any other geographical representation in this paper. While Copernicus Publications makes every effort to include appropriate place names, the final responsibility lies with the authors. Views expressed in the text are those of the authors and do not necessarily reflect the views of the publisher.

Acknowledgements

Thank you to Paris Good, Andrew Zolli and Brittany Zajic for their operational support and for ensuring the Basemap data were top quality. Allison Wolf and Kevin Farnham led the user engagement research that illuminated critical data needs within the fire modeling community, and PresencePG led the web application development. Thank you to Pat Manley for advancing the integration of data-driven approaches into resilient landscape design.

Financial support

Funding for the California Forest Observatory was provided by the Gordon and Betty Moore Foundation through Agreement #GMBF8741, by the California Tahoe Conservancy through Agreement #CTA19022R, and by the Tahoe Fund through Agreement #20190829.

Review statement

The review statement will be added by Copernicus Publications listing the handling editor as well as all contributing referees according to their status anonymous or identified.

References

Anderson, C.: Earthlib: a spectral library for continuous satellite land cover mapping, , https://doi.org/10.5281/ZENODO.18343900, 2026.

Anderson, C. and Marvin, D.: California Forest Observatory: Statewide Forest Monitoring Data, https://doi.org/10.1594/PANGAEA.989871, 2026.

Anderson, C., Joseph, M., Söthe, C., De Souza Mendes, F., Maschler, T., McCarthy, R., Mascaro, J., O'Shea, T., Rosenthal, A., and Marvin, D.: Forest Carbon Diligence: Digital MRV for Jurisdictional and Voluntary Offsets Markets, https://doi.org/10.32942/X2KW7H, 11 August 2025.

Anderson, C. B.: Biodiversity monitoring, earth observations and the ecology of scale, Ecol. Lett., 21, 1572–1585, https://doi.org/10.1111/ele.13106, 2018.

Asner, G. P.: Biophysical and Biochemical Sources of Variability in Canopy Reflectance, Remote Sens. Environ., 64, 234–253, https://doi.org/10.1016/s0034-4257(98)00014-5, 1998.

Asner, G. P. and Heidebrecht, K. B.: Spectral unmixing of vegetation, soil and dry carbon cover in arid regions: Comparing multispectral and hyperspectral observations, Int. J. Remote Sens., 23, 3939–3958, https://doi.org/10.1080/01431160110115960, 2002.

Badgley, G., Freeman, J., Hamman, J. J., Haya, B., Trugman, A. T., Anderegg, W. R. L., and Cullenward, D.: Systematic over-crediting in California's forest carbon offsets program, Glob. Change Biol., 28, 1433–1445, https://doi.org/10.1111/gcb.15943, 2022.

Bakker, K.: Gaia's Web: How Digital Environmentalism Can Combat Climate Change, Restore Biodiversity, Cultivate Empathy, and Regenerate the Earth, MIT Press, 289 pp., 2024.

Baron, J. N., Hessburg, P. F., Parisien, M.-A., Greene, G. A., Gergel, Sarah. E., and Daniels, L. D.: Fuel types misrepresent forest structure and composition in interior British Columbia: a way forward, Fire Ecol., 20, 15, https://doi.org/10.1186/s42408-024-00249-z, 2024.

Bateson, C. A., Asner, G. P., and Wessman, C. A.: Endmember bundles: a new approach to incorporating endmember variability into spectral mixture analysis, IEEE Trans. Geosci. Remote Sens., 38, 1083–1094, https://doi.org/10.1109/36.841987, 2000.

Bowman, D. M. J. S., Kolden, C. A., Abatzoglou, J. T., Johnston, F. H., van der Werf, G. R., and Flannigan, M.: Vegetation fires in the Anthropocene, Nat. Rev. Earth Environ., 1, 500–515, https://doi.org/10.1038/s43017-020-0085-3, 2020.

Brodrick, P. G., Davies, A. B., and Asner, G. P.: Uncovering Ecological Patterns with Convolutional Neural Networks, Trends Ecol. Evol., 34, 734–745, https://doi.org/10.1016/j.tree.2019.03.006, 2019.

Fire Perimeters: https://www.fire.ca.gov/what-we-do/fire-resource-assessment-program/fire-perimeters, last access: 20 January 2026.

California Air Resources Board: 2022 Scoping Plan for Achieving Carbon Neutrality, 2022.

California Department of Water Resources: 2020 Statewide Crop Mapping GIS Geodatabase, 2020.

Chamberlain, C. P., Cova, G. R., Kane, V. R., Cansler, C. A., Kane, J. T., Bartl-Geller, B. N., van Wagtendonk, L., Jeronimo, S. M. A., Stine, P., and North, M. P.: Sierra Nevada reference conditions: A dataset of contemporary reference sites and corresponding remote sensing-derived forest structure metrics for yellow pine and mixed-conifer forests, Data Brief, 51, 109807, https://doi.org/10.1016/j.dib.2023.109807, 2023.

Chang, T., Ndegwa, K., Gros, A., Landau, V. A., Zachmann, L. J., State, B., Gritts, M. A., Miller, C. W., Rutenbeck, N. E., Conway, S., and Bayes, G.: VibrantVS: A High-Resolution Vision Transformer for Forest Canopy Height Estimation, Remote Sens., 17, 1017, https://doi.org/10.3390/rs17061017, 2025.

Chave, J.: The problem of pattern and scale in ecology: what have we learned in 20 years?, Ecol. Lett., 16 Suppl 1, 4–16, https://doi.org/10.1111/ele.12048, 2013.

Coffield, S. R., Vo, C. D., Wang, J. A., Badgley, G., Goulden, M. L., Cullenward, D., Anderegg, W. R. L., and Randerson, J. T.: Using remote sensing to quantify the additional climate benefits of California forest carbon offset projects, Glob. Change Biol., 28, 6789–6806, https://doi.org/10.1111/gcb.16380, 2022.

https://doi.org/10.5194/essd-2026-255
Preprint. Discussion started: 20 July 2026

Combal, B., Baret, F., Weiss, M., Trubuil, A., Macé, D., Pragnère, A., Myneni, R., Knyazikhin, Y., and Wang, L.: Retrieval of canopy biophysical variables from bidirectional reflectance: Using prior information to solve the ill-posed inverse problem, Remote Sens. Environ., 84, 1–15, https://doi.org/10.1016/S0034-4257(02)00035-4, 2003.

Delheimer, M. S., Moriarty, K. M., Munro, H. L., Early, D. A., Hamm, K. A., and Green, R. E.: Structural complexity characterizes fine-scale forest conditions used by Pacific martens, J. Wildl. Manag., 87, e22388, https://doi.org/10.1002/jwmg.22388, 2023.

Diffenbaugh, N. S., Swain, D. L., and Touma, D.: Anthropogenic warming has increased drought risk in California, Proc. Natl. Acad. Sci. U. S. A., 112, 3931–3936, https://doi.org/10.1073/pnas.1422385112, 2015.

Gorelick, N., Hancher, M., Dixon, M., Ilyushchenko, S., Thau, D., and Moore, R.: Google Earth Engine: Planetary-scale geospatial analysis for everyone, Remote Sens. Environ., 202, 18–27, https://doi.org/10.1016/j.rse.2017.06.031, 2017.

Gustafson, M. L., McGinn, K., Heys, J. A., Sawyer, S. C., and Wood, C. M.: Rapid implementation and adaptive design of a large-scale monitoring program for a declining species, Biol. Conserv., 311, 111442, https://doi.org/10.1016/j.biocon.2025.111442, 2025.

Hack, B., Cansler, C. A., Peery, M. Z., and Wood, C. M.: Fine-scale forest structure, not management regime, drives occupancy of a declining songbird, the Olive-sided Flycatcher, in the core of its range, Ornithol. Appl., 126, duad065, https://doi.org/10.1093/ornithapp/duad065, 2024.

Hansen, M. C., Potapov, P. V., Moore, R., Hancher, M., Turubanova, S. A., Tyukavina, A., Thau, D., Stehman, S. V., Goetz, S. J., Loveland, T. R., Kommareddy, A., Egorov, A., Chini, L., Justice, C. O., and Townshend, J. R. G.: High-resolution global maps of 21st-century forest cover change, Science, 342, 850–853, https://doi.org/10.1126/science.1244693, 2013.

Heinz, D. C. and Chein-I-Chang: Fully constrained least squares linear spectral mixture analysis method for material quantification in hyperspectral imagery, IEEE Trans. Geosci. Remote Sens., 39, 529–545, https://doi.org/10.1109/36.911111, 2001.

Hendershot, J. N., Estes, B. L., and Wilson, K. N.: High-Resolution Forest Structure Mapping with Deep Learning to Evaluate Restoration Outcomes, Remote Sens., 18, 346, https://doi.org/10.3390/rs18020346, 2026.

Herbert, C., Haya, B. K., Stephens, S. L., and Butsic, V.: Managing nature-based solutions in fire-prone ecosystems: Competing management objectives in California forests evaluated at a landscape scale, Front. For. Glob. Change, 5, 957189, https://doi.org/10.3389/ffgc.2022.957189, 2022.

Isenburg, M.: LAStools: efficient LiDAR processing software, 2019.

Ishii, H. T., Jennings, G. M., Sillett, S. C., and Koch, G. W.: Hydrostatic constraints on morphological exploitation of light in tall Sequoia sempervirens trees, Oecologia, 156, 751–763, https://doi.org/10.1007/s00442-008-1032-z, 2008.

Jacquemoud, S., Bacour, C., Poilvé, H., and Frangi, J.-P.: Comparison of Four Radiative Transfer Models to Simulate Plant Canopies Reflectance: Direct and Inverse Mode, Remote Sens. Environ., 74, 471–481, https://doi.org/10.1016/S0034-4257(00)00139-5, 2000.

Jeronimo, S. M. A., Kane, V. R., Churchill, D. J., Lutz, J. A., North, M. P., Asner, G. P., and Franklin, J. F.: Forest structure and pattern vary by climate and landform across active-fire landscapes in the montane Sierra Nevada, For. Ecol. Manag., 437, 70–86, https://doi.org/10.1016/j.foreco.2019.01.033, 2019.

Joshi, N., Mitchard, E. T. A., Brolly, M., Schumacher, J., Fernández-Landa, A., Johannsen, V. K., Marchamalo, M., and Fensholt, R.: Understanding ‘saturation’ of radar signals over forests, Sci. Rep., 7, 3505, https://doi.org/10.1038/s41598-017-03469-3, 2017.

Kari Marie Norgaard: The Politics of Fire and the Social Impacts of Fire Exclusion on the Klamath, Humboldt J. Soc. Relat., 36, 77–101, 2014.

Kattenborn, T., Leitloff, J., Schiefer, F., and Hinz, S.: Review on Convolutional Neural Networks (CNN) in vegetation remote sensing, ISPRS J. Photogramm. Remote Sens. Off. Publ. Int. Soc. Photogramm. Remote Sens., 173, 24–49, https://doi.org/10.1016/j.isprsjprs.2020.12.010, 2021.

Keane, R. E.: Describing wildland surface fuel loading for fire management: a review of approaches, methods and systems, Int. J. Wildland Fire, 22, 51–62, https://doi.org/10.1071/WF11139, 2013.

Keane, R. E., Reinhardt, E. D., Scott, J., Gray, K., and Reardon, J.: Estimating forest canopy bulk density using six indirect methods, Can. J. For. Res. J. Can. Rech. For., 35, 724–739, https://doi.org/10.1139/x04-213, 2005.

Kingma, D. P. and Ba, J.: Adam: A Method for Stochastic Optimization, 2014.

Konings, A. G., Rao, K., and Steele-Dunne, S. C.: Macro to micro: microwave remote sensing of plant water content for physiology and ecology, New Phytol., 223, 1166–1172, https://doi.org/10.1111/nph.15808, 2019.

Kramer, H. A., Collins, B. M., Kelly, M., and Stephens, S. L.: Quantifying Ladder Fuels: A New Approach Using LiDAR, For. Trees Livelihoods, 5, 1432–1453, https://doi.org/10.3390/f5061432, 2014.

Kramer, H. A., Collins, B. M., Lake, F. K., Jakubowski, M. K., Stephens, S. L., and Kelly, M.: Estimating Ladder Fuels: A New Approach Combining Field Photography with LiDAR, Remote Sens., 8, 766, https://doi.org/10.3390/rs8090766, 2016.

Kramer, H. A., Kelly, K. G., Whitmore, S. A., Berigan, W. J., Reid, D. S., Wood, C. M., Klinck, H., Kahl, S., Manley, P. N., Sawyer, S. C., and Peery, M. Z.: Using bioacoustics to enhance the efficiency of spotted owl surveys and facilitate forest restoration, J. Wildl. Manag., 88, e22533, https://doi.org/10.1002/jwmg.22533, 2024.

LANDFIRE: FBFM40, 2016a.

LANDFIRE: Forest Canopy Bulk Density, 2016b.

Langhans, K. E., Echeverri, A., Xu, M., Callahan, M., Palmeri, M. L., Nguyen, O., Ardoin, N. M., and Daily, G. C.: Urban community gardens foster positive human-avian interactions across an income gradient in San Francisco, Landsc. Urban Plan., 261, 105391, https://doi.org/10.1016/j.landurbplan.2025.105391, 2025.

Levin, S. A.: The problem of pattern and scale in ecology: The Robert H. macarthur award lecture, Ecology, 73, 1943–1967, https://doi.org/10.2307/1941447, 1992.

Li, S. and Banerjee, T.: Spatial and temporal pattern of wildfires in California from 2000 to 2019, Sci. Rep., 11, 8779, https://doi.org/10.1038/s41598-021-88131-9, 2021.

Linley, G. D., Jolly, C. J., Doherty, T. S., Geary, W. L., Armenteras, D., Belcher, C. M., Bliege Bird, R., Duane, A., Fletcher, M., Giorgis, M. A., Haslem, A., Jones, G. M., Kelly, L. T., Lee, C. K. F., Nolan, R. H., Parr, C. L., Pausas, J. G., Price, J. N., Regos, A., Ritchie, E. G., Ruffault, J., Williamson, G. J., Wu, Q., and Nimmo, D. G.: What do you mean, ‘megafire’?, Glob. Ecol. Biogeogr., 31, 1906–1922, https://doi.org/10.1111/geb.13499, 2022.

https://doi.org/10.5194/essd-2026-255
Preprint. Discussion started: 20 July 2026

Malenovský, Z., Rott, H., Cihlar, J., Schaepman, M. E., García-Santos, G., Fernandes, R., and Berger, M.: Sentinels for science: Potential of Sentinel-1, -2, and -3 missions for scientific observations of ocean, cryosphere, and land, Remote Sens. Environ., 120, 91–101, https://doi.org/10.1016/j.rse.2011.09.026, 2012.

Manley, P. N., Povak, N. A., Wilson, K. N., Fairweather, M. L., Griffey, V., and Long, L. L.: Blueprint for resilience: the Tahoe-Central Sierra Initiative, U.S. Department of Agriculture, Forest Service, Pacific Southwest Research Station, Albany, CA, https://doi.org/10.2737/PSW-GTR-277, 2023.

Marks-Block, T. A.: Karuk and Yurok prescribed cultural fire revitalization in California's Klamath Basin: socio-ecological dynamics and political ecology of indigenous burning and resource management, edited by: Curran, L. M., Ebron, P. A., and Wilcox, M., [Stanford University], [Stanford, California], 2020.

Martin-Ducup, O., Dupuy, J.-L., Soma, M., Guerra-Hernandez, J., Marino, E., Fernandes, P. M., Just, A., Corbera, J., Toutchkov, M., Sorribas, C., Bock, J., Piboule, A., Pirotti, F., and Pimont, F.: Unlocking the potential of Airborne LiDAR for direct assessment of fuel bulk density and load distributions for wildfire hazard mapping, Agric. For. Meteorol., 362, 110341, https://doi.org/10.1016/j.agrformet.2024.110341, 2025.

Marvin, D. C., Koh, L. P., Lynam, A. J., Wich, S., Davies, A. B., Krishnamurthy, R., Stokes, E., Starkey, R., and Asner, G. P.: Integrating technologies for scalable ecology and conservation, Glob. Ecol. Conserv., 7, 262–275, https://doi.org/10.1016/j.gecco.2016.07.002, 2016.

McCormick, N. J.: Inverse Radiative Transfer Problems: A Review, Nucl. Sci. Eng. J. Am. Nucl. Soc., 112, 185–198, https://doi.org/10.13182/NSE112-185, 1992.

McIntyre, P. J., Thorne, J. H., Dolanc, C. R., Flint, A. L., Flint, L. E., Kelly, M., and Ackerly, D. D.: Twentieth-century shifts in forest structure in California: Denser forests, smaller trees, and increased dominance of oaks, Proc. Natl. Acad. Sci. U. S. A., 112, 1458–1463, https://doi.org/10.1073/pnas.1410186112, 2015.

Mietkiewicz, N., Balch, J. K., Schoennagel, T., Leyk, S., St. Denis, L. A., and Bradley, B. A.: In the Line of Fire: Consequences of Human-Ignited Wildfires to Homes in the U.S. (1992–2015), Fire, 3, 50, https://doi.org/10.3390/fire3030050, 2020.

Mooney, H. A., Parsons, D. J., and Kummerow, J.: Plant Development in Mediterranean Climates, in: Phenology and Seasonality Modeling, edited by: Lieth, H., Springer Berlin Heidelberg, Berlin, Heidelberg, 255–267, https://doi.org/10.1007/978-3-642-51863-8_22, 1974.

Moreno-Martínez, Á., Camps-Valls, G., Kattge, J., Robinson, N., Reichstein, M., van Bodegom, P., Kramer, K., Cornelissen, J. H. C., Reich, P., Bahn, M., Niinemets, Ü., Peñuelas, J., Craine, J. M., Cerabolini, B. E. L., Minden, V., Laughlin, D. C., Sack, L., Allred, B., Baraloto, C., Byun, C., Soudzilovskaia, N. A., and Running, S. W.: A methodology to derive global maps of leaf traits using remote sensing and climate data, Remote Sens. Environ., 218, 69–88, https://doi.org/10.1016/j.rse.2018.09.006, 2018.

Mutanga, O., Masenyama, A., and Sibanda, M.: Spectral saturation in the remote sensing of high-density vegetation traits: A systematic review of progress, challenges, and prospects, ISPRS J. Photogramm. Remote Sens., 198, 297–309, https://doi.org/10.1016/j.isprsjprs.2023.03.010, 2023.

Myers, N., Mittermeier, R. A., Mittermeier, C. G., da Fonseca, G. A., and Kent, J.: Biodiversity hotspots for conservation priorities, Nature, 403, 853–858, https://doi.org/10.1038/35002501, 2000.

Ndegwa, K., Gros, A., Chang, T., Diaz, D., Landau, V. A., Rutenbeck, N. E., Zachmann, L. J., Bayes, G., and Conway, S.: VibrantSR: Sub-Meter Canopy Height Models from Sentinel-2 Using Generative Flow Matching, https://doi.org/10.48550/arXiv.2601.09866, 14 January 2026.

Ochoa, F., Brodrick, P. G., Okin, G. S., Ben-Dor, E., Meyer, T., Thompson, D. R., and Green, R. O.: Soil and vegetation cover estimation for global imaging spectroscopy using spectral mixture analysis, Remote Sens. Environ., 324, 114746, https://doi.org/10.1016/j.rse.2025.114746, 2025.

OpenStreetMap contributors: OpenStreetMap Data, 2019.

Pacific Gas & Electric: 2023-2025 Wildfire Mitigation Plan R5, 2024.

Pascual, A., Guerra-Hernández, J., Botequim, B., and González-Ferreiro, E.: Supporting fire behavior modelling with canopy base height and canopy bulk density estimates using airborne and spaceborne lidar, Ecol. Inform., 94, 103612, https://doi.org/10.1016/j.ecoinf.2026.103612, 2026.

Planet Labs PBC Team: Planet Application Program Interface: In Space for Life on Earth, 2020.

Reinhardt, E., Lutes, D., and Scott, J.: FuelCalc: A method for estimating fuel characteristics, in: In: Andrews, Patricia L.; Butler, Bret W., comps. 2006. Fuels Management-How to Measure Success: Conference Proceedings. 28-30 March 2006; Portland, OR. Proceedings RMRS-P-41. Fort Collins, CO: US Department of Agriculture, Forest Service, Rocky Mountain Research Station. p. 273-282, 2006.

Rollins, M. G.: LANDFIRE: a nationally consistent vegetation, wildland fire, and fuel assessment, Int. J. Wildland Fire, 18, 235–249, https://doi.org/10.1071/WF08088, 2009.

Ronneberger, O., Fischer, P., and Brox, T.: U-Net: Convolutional Networks for Biomedical Image Segmentation, in: Medical Image Computing and Computer-Assisted Intervention – MICCAI 2015, vol. 9351, edited by: Navab, N., Hornegger, J., Wells, W. M., and Frangi, A. F., Springer International Publishing, Cham, 234–241, https://doi.org/10.1007/978-3-319-24574-4_28, 2015.

Salter, J. F.: White Paper on Behalf of the Karuk Tribe of California, Context Statement Eff. Klamath Hydroelectr. Proj. Tradit. Resour. Uses Cult. Patterns Karuk People Klamath River Corridor, 1–82, 2003.

Schoennagel, T., Balch, J. K., Brenkert-Smith, H., Dennison, P. E., Harvey, B. J., Krawchuk, M. A., Mietkiewicz, N., Morgan, P., Moritz, M. A., Rasker, R., Turner, M. G., and Whitlock, C.: Adapt to more wildfire in western North American forests as climate changes, Proc. Natl. Acad. Sci. U. S. A., 114, 4582–4590, https://doi.org/10.1073/pnas.1617464114, 2017.

Schulte to Bühne, H. and Pettorelli, N.: Better together: Integrating and fusing multispectral and radar satellite imagery to inform biodiversity monitoring, ecological research and conservation science, Methods Ecol. Evol. Br. Ecol. Soc., 9, 849–865, https://doi.org/10.1111/2041-210X.12942, 2018.

Scott, J. H.: Assessing Crown Fire Potential by Linking Models of Surface and Crown Fire Behavior, U.S. Department of Agriculture, Forest Service, Rocky Mountain Research Station, 2001.

Scott, J. H. and Burgan, R. E.: Standard Fire Behavior Fuel Models: A Comprehensive Set for Use with Rothermel's Surface Fire Spread Model, US Department of Agriculture, Forest Service, Rocky Mountain Research Station, 2005.

Singh, M., Ong, A., and Sud, R.: Wires and fire: Wildfire investment and network cost differences across California's power providers, Electr. J., 38, 107475, https://doi.org/10.1016/j.tej.2025.107475, 2025.

https://doi.org/10.5194/essd-2026-255
Preprint. Discussion started: 20 July 2026

Stephens, S. L., Collins, B. M., Fettig, C. J., Finney, M. A., Hoffman, C. M., Knapp, E. E., North, M. P., Safford, H., and Wayman, R. B.: Drought, Tree Mortality, and Wildfire in Forests Adapted to Frequent Fire, Bioscience, 68, 77–88, https://doi.org/10.1093/biosci/bix146, 2018.

Turubanova, S., Potapov, P., Hansen, M. C., Li, X., Tyukavina, A., Pickens, A. H., Hernandez-Serna, A., Arranz, A. P., Guerra-Hernandez, J., Senf, C., Häme, T., Valbuena, R., Eklundh, L., Brovkina, O., Navrátilová, B., Novotný, J., Harris, N., and Stolle, F.: Tree canopy extent and height change in Europe, 2001–2021, quantified using Landsat data archive, Remote Sens. Environ., 298, 113797, https://doi.org/10.1016/j.rse.2023.113797, 2023.

US Environmental Protection Agency: Level III Ecoregions of the Continental United States, US EPA - National Health and Environmental Effects Research Laboratory, Corvalis, OR, 2013.

US Geological Survey: USGS 3D Elevation Program Lidar Point Clouds, 2019.

Van Wagner, C. E.: Conditions for the start and spread of crown fire, Can. J. For. Res. J. Can. Rech. For., 7, 23–34, https://doi.org/10.1139/x77-004, 1977.

Wagner, F. H., Roberts, S., Ritz, A. L., Carter, G., Dalagnol, R., Favrichon, S., Hirye, M. C. M., Brandt, M., Ciais, P., and Saatchi, S.: Sub-meter tree height mapping of California using aerial images and LiDAR-informed U-Net model, Remote Sens. Environ., 305, 114099, https://doi.org/10.1016/j.rse.2024.114099, 2024.

Wang, Z., Wara, M., Majumdar, A., and Rajagopal, R.: Local and utility-wide cost allocations for a more equitable wildfire-resilient distribution grid, Nat. Energy, 8, 1097–1108, https://doi.org/10.1038/s41560-023-01306-8, 2023.

Watson, W. A., Hofstadter, D. F., Jones, G. M., Kramer, H. A., Kryshak, N. F., Zulla, C. J., Whitmore, S. A., O'Rourke, V., Keane, J. J., Gutiérrez, R. J., and Peery, M. Z.: Characterizing juvenile dispersal dynamics of invasive Barred Owls: Implications for management, Ornithol. Appl., 126, duad061, https://doi.org/10.1093/ornithapp/duad061, 2024.

Went, F. W.: The Ecology of Desert Plants, Sci. Am., 192, 68–76, 1955.

Wessman, C. A., Bateson, C. A., and Benning, T. L.: Detecting Fire and Grazing Patterns in Tallgrass Prarie Using Spectral Mixture Analysis, Ecol. Appl., 7, 493–511, https://doi.org/10.1890/1051-0761(1997)007%5B0493:DFAGPI%5D2.0.CO;2, 1997.

Wiens, J. A.: Spatial Scaling in Ecology, Funct. Ecol., 3, 385–397, https://doi.org/10.2307/2389612, 1989.

Wilkinson, Z. A., Kramer, H. A., Jones, G. M., Zulla, C. J., McGinn, K., Barry, J. M., Sawyer, S. C., Tanner, R., Gutiérrez, R. J., Keane, J. J., and Peery, M. Z.: Tall, heterogeneous forests improve prey capture, delivery to nestlings, and reproductive success for Spotted Owls in southern California, Ornithol. Appl., 125, duac048, https://doi.org/10.1093/ornithapp/duac048, 2023.

Wolff, A., Farnham, K., Marvin, D. C., and Anderson, C. B.: Ethnography synthesis: Findings from qualitative research, Salo Sciences Inc., San Francisco, CA, 2020.

Yao, M., Bharadwaj, M., Zhang, Z., Jin, B., and Callaway, D. S.: Predicting electricity infrastructure induced wildfire risk in California, Environ. Res. Lett., 17, 094035, https://doi.org/10.1088/1748-9326/ac8d18, 2022.

Young-Hart, L., Stine, P., Manley, P., and Clark, C.: Sierra Nevada Regional Resource Kit Metric Dictionary, 2024.

https://doi.org/10.5194/essd-2026-255
Preprint. Discussion started: 20 July 2026

Zeng, Y., Chen, X., Zhang, Y., Bai, L., and Han, J.: Dense-U-Net: densely connected convolutional network for semantic segmentation with a small number of samples, in: Tenth International Conference on Graphics and Image Processing (ICGIP 2018), 110692B, https://doi.org/10.1117/12.2524406, 2019.

Zhu, X. X., Xiong, Z., Wang, Y., Stewart, A. J., Heidler, K., Wang, Y., Yuan, Z., Dujardin, T., Xu, Q., and Shi, Y.: On the foundations of Earth foundation models, Commun. Earth Environ., 7, 103, https://doi.org/10.1038/s43247-025-03127-x, 2026.

Zulla, C. J., Jones, G. M., Kramer, H. A., Keane, J. J., Roberts, K. N., Dotters, B. P., Sawyer, S. C., Whitmore, S. A., Berigan, W. J., Kelly, K. G., Gutiérrez, R. J., and Peery, M. Z.: Forest heterogeneity outweighs movement costs by enhancing hunting success and reproductive output in California spotted owls, Landsc. Ecol., 38, 2655–2673, https://doi.org/10.1007/s10980-023-01737-4, 2023.